Geophysical Research Letters

RESEARCH LETTER
10.1029/2019GL083017

Experimental Constraints on an MgO Exsolution-Driven Geodynamo

Zhixue Du[1], Asmaa Boujibar[2], Peter Driscoll[3], and Yingwei Fei[2]

[1]State key Laboratory of Isotope Geochemistry, Guangzhou Institute of Geochemistry, Chinese Academy of Sciences, Guangzhou, China, [2]Geophysical Laboratory, Carnegie Institution of Washington, Washington, DC, USA, [3]Department of Terrestrial Magnetism, Carnegie Institution of Washington, Washington, DC, USA

Key Points:
- We have conducted new experiments on Mg partitioning into Fe alloy at high pressures
- Effect of temperature on Mg partitioning is weak, but the role of oxygen in Fe alloy is strong
- MgO exsolution is limited and can power an early geodynamo only if the core cools rapidly

Supporting Information:
- Supporting Information S1
- Data Set S1

Correspondence to:
Z. Du,
duzhixue@gig.ac.cn

Citation:
Du, Z., Boujibar, A., Driscoll, P., & Fei, Y. (2019). Experimental constraints on an MgO exsolution-driven geodynamo. *Geophysical Research Letters*, *46*, 7379–7385. https://doi.org/10.1029/2019GL083017

Received 9 APR 2019
Accepted 11 JUN 2019
Accepted article online 18 JUN 2019
Published online 11 JUL 2019

Abstract MgO exsolution has been proposed to drive an early geodynamo. Experimental studies, however, have drawn different conclusions regarding the applicability of MgO exsolution. While many studies suggest that significant Mg can dissolve into the Earth's core, the amount of MgO exsolved out of the core, which hinges on the temperature dependence of MgO solubility, remains unclear. Here we present new high-temperature experiments to better constrain the temperature and compositional dependence of Mg partitioning between Fe alloys and silicate liquids. Our experiments show that Mg partitioning is weakly dependent on temperature, while confirming its strong dependence on oxygen content in Fe alloys. This implies that MgO exolution is limited as the core cools but can help drive an early geodyanamo if the core heat loss is slightly subadiabatic. If an exosolution-driven geodynamo did occur, it was likely over a limited time span that depends on the core thermal history and conductivity.

Plain Language Summary The existence of Earth's magnetic field has been dated back to at least 3.5 billion years ago. Yet its origin is under intense debates. A recent hypothesis is that abundant MgO, a major component of the Earth's mantle, may exsolve out of the Earth's core, providing energy to generate long-lasting magnetic field. However, how much MgO can exsolve out of the core is still poorly constrained. Here we conduct new high-pressure experiments to study the geochemical behavior of MgO under the Earth's core conditions. We find that the solubility of MgO in the Earth's core is weakly dependent on temperature. This suggests that the exsolution of MgO as the core cools is limited and can only power the geodynamo over a relatively limited time. Thus, the continuous operation of the Earth's ancient magnetic field remains a mystery.

1. Introduction

The existence of an early geodynamo has been found going back to at least 3.5 Ga as indicated by the paleomagnetic signature of ancient rocks (Biggin et al., 2015; Tarduno et al., 2015). The energy sources, however, that powered such an early geodynamo are hotly debated (e.g., Olson, 2013). Thermal convection associated with core cooling may be insufficient in light of recent upward revisions to the thermal conductivity of the Earth's core (e.g., Konopkova et al., 2016; Ohta et al., 2016; Pozzo et al., 2012). Compositional convection associated with the solidification of the inner core was likely unavailable over much of this time because the inner core is thought to be significantly younger (~0.5–1 Ga) than the oldest paleomagnetic evidence (e.g., Driscoll, 2016; Labrosse et al., 2001).

Recently, the gravitational energy released by MgO exsolution has been hypothesized as a possible buoyancy source to drive the early geodynamo (O'Rourke & Stevenson, 2016). Follow-up experimental studies confirmed that significant MgO may be dissolved into the core during late-stage high-energy impacts (Badro et al., 2016; Du et al., 2017). Yet discrepancy exists in how much MgO can be exsolved during core cooling, questioning the viability of this mechanism. Discrepancy in the exsolution rate is mainly due to challenges in constraining temperature dependence of Mg partitioning between Fe alloy and silicate liquid. This is due, in part, to the limited temperature range of 3000–5500 K of the experiments (e.g., Badro et al., 2018; Du et al., 2017). In order to better constrain this temperature dependence, we present new experiments extending to low temperatures of ~2000 K. We develop a thermodynamic model to describe the temperature, pressure, and compositional dependence of Mg solubility. Lastly, we will discuss the implications for generating the Earth's magnetic field.

2. Methods

We investigate metal-silicate interactions at high pressures and high temperatures using a multi-anvil press (supporting information). Chondrites (CI carbonaceous or EH4 enstatite chondrites; e.g., Wasson & Kallemeyn, 1988) and Fe-FeO-FeS alloy are chosen to represent the mantle and core compositions, respectively. Equilibrium is achieved at pressures from 3.5 to 8 GPa and temperatures from 1973 to 2173 K. Samples are temperature-quenched by turning off the electric power supply. Run products are subsequently dry polished with sand papers and alumina powder. Melting regions are identified by ex situ textural features of recovered run-products (Figure S1 of the supporting information). Chemical analysis is performed with a field-emission electron microprobe (supporting information). Two types of Fe alloys are observed to be immiscible in these experimental conditions, namely, S-rich Fe alloy and S-poor Fe alloy (Figure S1). The Mg concentrations in S-poor Fe alloys are below detection limit, primarily due to their low oxygen contents, as discussed below. Therefore, only the Mg measurements for S-rich Fe alloy are reported, shown in Table S1.

The exchange reaction of Mg between silicate liquid and Fe alloy may be expressed as follows:

$$\mathrm{MgO}^{\text{silicate liquid}} + \mathrm{Fe}^{\text{alloy}} \rightleftharpoons \mathrm{FeO}^{\text{silicate liquid}} + \mathrm{Mg}^{\text{alloy}} \quad (1)$$

The exchange coefficient is calculated as $K_{\mathrm{Mg}} = X_{\mathrm{FeO}}X_{\mathrm{Mg}}/(X_{\mathrm{Fe}}X_{\mathrm{MgO}})$. Molar compositions of silicate liquid and iron alloy are given as X_{FeO}, X_{MgO}, X_{Mg}, and X_{Fe}, respectively. Alternative reactions, such as dissociation and dissolution reactions ($R2$ and $R3$, respectively, in the supporting information) are also proposed to describe how Mg is dissolved in Fe alloy (Badro et al., 2018; Du et al., 2017). For simplicity, we will focus on exchange reaction ($R1$) to describe our experimental results and discuss possibilities of other reactions in section 4 and 5.

3. Data

The measured K_{Mg} values are plotted as red circles in Figure 1, along with previous experimental results in blue symbols (Badro et al., 2018; Badro et al., 2016; Chidester et al., 2017; Du et al., 2017; Jackson et al., 2018; Suer et al., 2017). K_{Mg} values span ~3 orders of magnitude, nearly covering the ranges of previous studies. This large range of K_{Mg} is striking, given the limited range of pressure and temperature (3–8 GPa and 1973–2173 K), compared with the much wider ranges of 20–138 GPa and 3000–5500 K reported in previous studies (Figure 1a). We then plot our results as a function of oxygen's mole fraction in the Fe alloy (X_{O}), shown in Figure 1b. Interestingly, our results define a clear positive correlation between K_{Mg} and X_{O}. This suggests an important role of oxygen controlling Mg partitioning behavior, consistent with previous studies (Badro et al., 2018; Du et al., 2017). Taking all available data into account, this trend is still evident but with more scatters. This indicates other factors, besides X_{O} are also affecting K_{Mg}. Our present data are limited in temperature and pressure, therefore separating oxygen effect from other effects on Mg partitioning. Once the oxygen effect is determined, we can then combine our results with previous results at higher temperature and pressures, further constraining the effect of temperature, pressure, and other compositional terms. Alternatively, in order to identify and quantify all controlling factors, we constructed the following thermodynamic model, taking into account the effects of pressure, temperature, and the interactions between Mg and the light elements in the Fe alloys (see below).

4. Results

Similar to the approach by Du et al. (2017), K_{Mg} may be expressed as a function of temperature (T, kelvin), pressure (P, GPa), and the composition of Fe alloy (X_i, the mole fraction of elements i (O, Si, C, S)), as follows:

$$\log_{10}\left(K_{\mathrm{Mg}}\right) = a + b/T + cP/T + d\ \log_{10}(1-X_{\mathrm{O}}) + e\ \log_{10}(1-X_{\mathrm{Si}}) + f\ \log_{10}(1-X_{\mathrm{C}}) + g\ \log_{10}(1-X_{\mathrm{S}})$$

where a–g are fitting parameters. We conducted a stepwise, nonweighted least squares regression to our "combined" data set, including this study and previous studies (Badro et al., 2018; Badro et al., 2016; Chidester et al., 2017; Du et al., 2017; Jackson et al., 2018; Suer et al., 2017). We find $a = -3.0 \pm 0.26$, $b = -2314 \pm 662$, $c = 26 \pm 10$, $d = -10 \pm 0.9$, $e = 1.6 \pm 0.3$, with $R^2 = 0.77$. Quoted uncertainties are

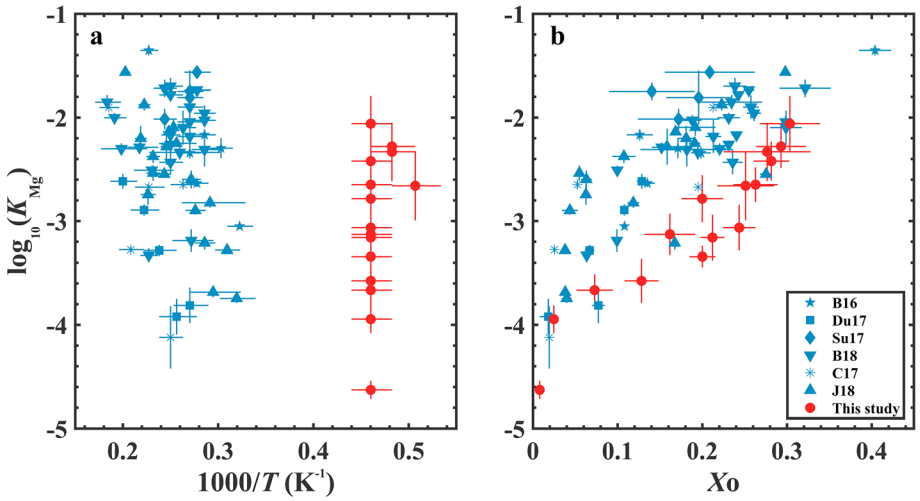

Figure 1. Temperature (a) and compositional (b) dependence of K_{Mg}. X_O is the mole fraction of oxygen in Fe alloy. Symbols of each study are shown in red circles (this study), stars (B16; Badro et al., 2016), squares (Du17; Du et al., 2017), diamonds (Su17; Suer et al., 2017), inverted triangles (B18; Badro et al., 2018), asterisks (C17; Chidester et al., 2017), and triangles (J18; Jackson et al., 2018). The 1σ error bars are plotted for uncertainties. See Table S1 for all experimental results in this study.

1σ errors. We find that terms for X_C and X_S are not significant at the 95% confidence threshold and therefore not included in the regression; that is, f and g are set to be zero. See also Table S2 for a list of fitted parameters and Figure 2 for a comparison between the experimental data (Observed) and our model predictions (Predicted).

Our results confirm the previous findings that K_{Mg} strongly depends on Xo, oxygen concentration in the Fe alloy (Du et al., 2017), evident from Figure 1b as discussed above. Du et al. (2017) did not constrain the temperature dependence of K_{Mg} due to limited data set. Our new results provide important constraints: moderate temperature and pressure control on K_{Mg}, namely, small b and c, for $1/T$ and P/T terms, respectively. This new empirical constrains differ from previously assumed strong temperature dependence (O'Rourke & Stevenson, 2016) when experimental results were unavailable. Badro et al. (2018) also found moderate temperature dependence of Mg partitioning, consistent with our results. We note that oxygen content in S-rich Fe alloy varies from 0.3 to 12.6 wt%, which is correlated with the FeO content in silicate melt (Kiseeva & Wood, 2013). Meanwhile, oxygen in sulfur-rich alloy controls the Mg partitioning (Figure 1b). So sulfur does not directly influence Mg partitioning, in agreement with our regression result, where parameter g is statistically insignificant. In our study, Mg content is below detection limit in S-poor Fe alloy, primarily due to its low oxygen contents, in agreement with previous findings (Badro et al., 2018; Du et al., 2017).

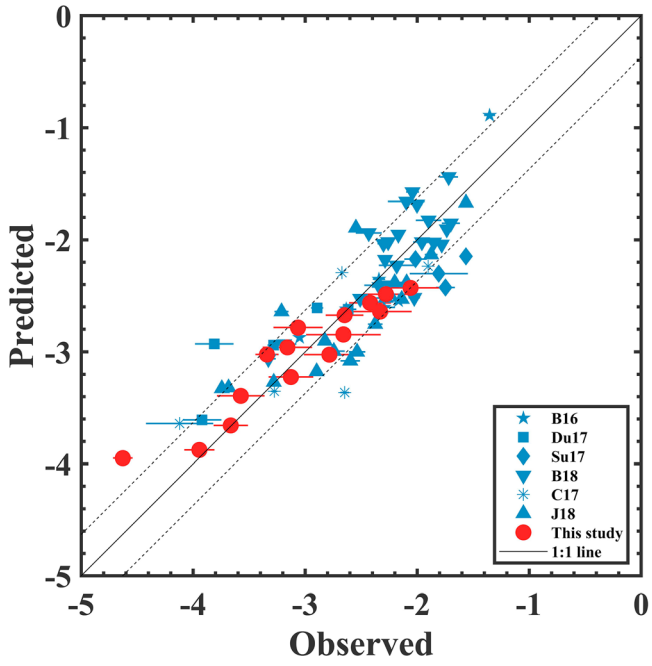

Figure 2. Comparisons of exchange coefficients $\log_{10}(K_{Mg})$ between experiments (Observed) and predictions from the best-fitted model (Predicted). Parameters of the best-fitted model are given in the text and listed in Table S2. Solid line is the 1:1 line, and dashed lines are ±0.37 log-unit 1σ errors.

It has been also suggested that Mg may be dissolved in Fe alloy as an MgO component, shown in dissolution reaction ($R3$, supporting information; Badro et al., 2018; Du et al., 2017). Our results agree with model predictions by Badro et al. (2018); Figures S2a and S2b). Similar to Badro et al. (2018), we find that dissociation ($R2$, supporting information) and dissolution ($R3$) yield greater value of R^2 ~ 0.97, compared to that of ~0.76 for exchange reaction ($R1$). Based on this criterion, $R2$ and $R3$ may better describe Mg (or MgO) speciation in iron-rich alloy (Badro et al., 2018). However, we also point out that R^2 should not be the only criterion to

judge the better or worse of thermodynamic models. Yet values of root mean square error are rather similar for all three reactions, in the range of ~0.31–0.37 (Tables S2 and S3, supporting information). Therefore, we consider that all models are viable mechanisms to describe the Mg speciation in Fe alloys. We will also show, as follows, that the calculated exsolution rates, regardless of the choices of thermodynamic models, yield similar results. This is, however, not surprising, given all models are based on the same data sets. Also, the model predictions are within the experiments' parameters space (namely, T, P, and compositions). Therefore, we elect to use exchange reaction ($R1$) as an example to illustrate MgO exsolution process and its implications on powering an early geodynamo.

5. Implications: MgO Exsolution During Core Cooling

Following the previous approach (Du et al., 2017; O'Rourke & Stevenson, 2016), we compute Mg solubility in the core using experimentally determined K_{Mg}. Mg can be dissolved in the impactors' core primarily during late-stage giant impacts (Badro et al., 2016; O'Rourke & Stevenson, 2016). Yet the physical conditions of these giant impacts are largely unknown (e.g., Nakajima & Stevenson, 2015). Therefore, we assume that the core is well mixed with an initial concentration of Mg (0–2 wt%), Si (3 wt%), and O (6 wt%; O'Rourke & Stevenson, 2016]. During core cooling, MgO-rich liquid is exsolved out at the top of the core. To give an upper limit to the possible exsolution rate, we choose the fitted parameters b and c on the higher end of their 1σ uncertainty (i.e., $b = -2900$, c=16), which gives an upper limit to the temperature dependence of K_{Mg}. In addition, 6 wt% O can be considered near the upper bound of possible oxygen content in the core (e.g., Badro et al., 2015; Fischer et al., 2015). Therefore, the calculated Mg solubility and exsolution rate can be considered as an upper limit.

Calculated core Mg solubility and exsolution rate at core mantle boundary (CMB) pressure are shown (red curves in Figure 3) as a function of temperatures, assuming exsolution as a liquid, along with previous results (black curves) (Du et al., 2017). We also show the results from O'Rourke & Stevenson, 2016, where K_{Mg} is assumed to be strongly temperature dependent. Model results, assuming dissolution reaction ($R3$) are also shown as dotted curves, where a core of 3 wt% Si and 6 wt% O is in equilibrium with a pyrolitic lowermost mantle (*Badro* et al., 2018).

Similar to a previous approach (Du et al., 2017), we illustrate exsolution process starting ~1.7 wt% Mg in the core (Figure 3a). When the core cools, Mg content drops along the red solid curve to ~1.5 wt% at the present day. O'Rourke and Stevenson (2016), assuming 2 wt% initial Mg, produces a core that is undersaturated in Mg until ~4750 K. Then the Mg content decrease along the dashed curve to a much smaller value ~0.7 wt%. Our results, along with previous results (Badro et al., 2018; Du et al., 2017), show a weaker temperature dependence of Mg solubility, changing by ~0.2 wt% from 5000 to 4000 K. This significantly limits MgO exsolution, in contrast to previous studies (O'Rourke & Stevenson, 2016). Mg content is estimated to be ~1.5 wt% in the present-day core. This should be treated as an upper bound, and its exact amount may be investigated by further geophysical observations, such as densities and sound speeds of the core. The main difference between our model and that of Badro et al. (2018) is that they calculate Mg solubility from equilibrium constant K_3 assuming MgO dissolution reaction (R3, supporting information). Both studies predict similar temperature dependence, although differing the absolute values. Clearly, the temperature dependences of Mg solubility is weak, for each of the thermodynamic models, $R1$, $R2$ or $R3$ (Figure S3, supporting information).

Our results show that an exsolution rate is four times lower than the minimum value of 2×10^{-5} K^{-1} estimated by O'Rourke and Stevenson (2017) and 10 times lower than the optimum value ($4–5 \times 10^{-5} K^{-1}$; Du et al., 2017; O'Rourke & Stevenson, 2017) required to power a geodynamo early in Earth's history. Badro et al. (2018) obtained similar low exsolution rate (0.4×10^{-5} K^{-1}) assuming dissolution reaction ($R3$), consistent with our model predictions based on exchange reaction ($R1$). MgO exsolution can be an important source of buoyancy flux to drive fluid motion, thanks to its high efficiency of converting gravitational energy to kinetic energy (e.g., Du et al., 2017; Olson et al., 2017; O'Rourke & Stevenson, 2016).

To illustrate the contributions from thermal cooling and exsolution, we compute the buoyancy fluxes as a function of heat flow at the CMB (Q_{cmb}) as detailed in the supporting information. For simplicity, we

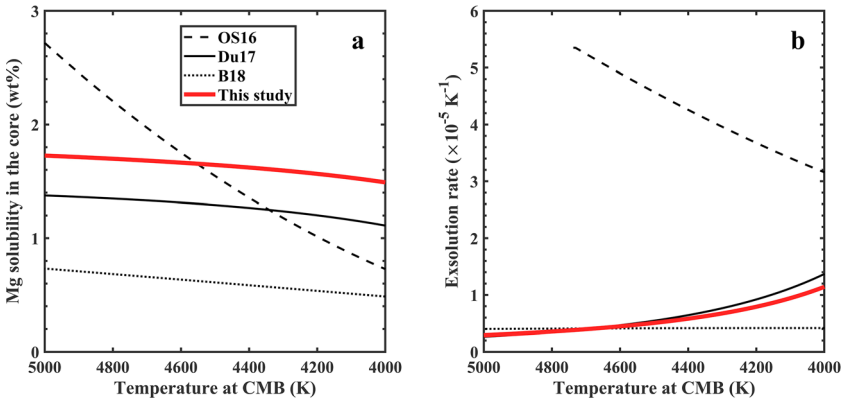

Figure 3. Calculated Mg solubility (a) and exsolution rate (b) at the Earth's core mantle boundary (CMB) pressure (136 GPa) as a function of CMB temperature, from this study (red) and Du17 (black; Du et al., 2017). Model result from B18 (Badro et al., 2018) is a dotted line, assuming the same Si (3 wt%) and O (6 wt%) content in the core. The core is assumed to be saturated with Mg after the core forms except in the study OS16 with initial Mg content of 2 wt% (O'Rourke & Stevenson, 2016). In our study, we shift the fitted parameters b and c by 1σ uncertainty (i.e., $b = -2{,}900$, $c = 16$) to the upper end of temperature dependence of K_{Mg}. Therefore, the calculated exsolution rate can be considered as an upper limit. The legend in (b) is identical with that in (a). Note that exsolution rates calculated from K_2, K_3, and K_{MgO} are similar to those from Badro et al. (2018), shown in Figure S3.

assume no radioactivity in the core (e.g., Chidester et al., 2017; Suer et al., 2017; Xiong et al., 2018) and no inner core growth so that Q_{cmb} equals the heat from secular cooling (Q_{sec}), which is proportional to the core cooling rate. We also adopt an adiabatic heat flow of $Q_{ad} = 12$ TW and average exsolution rate of ~0.6×10^{-5} K^{-1}. We find that for $Q_{cmb} < 9.2$ TW, the total buoyancy flux is negative; therefore, the core is stratified, and no dynamo is expected. For $9.2 \leq Q_{cmb} \leq 12.0$ TW, thermal buoyancy is subadiabatic, but the contribution from exsolution is enough to overcome thermal stratification to drive convection, denoted as the "exsolution" regime (green in Figure 4). Note that during the exsolution regime, the contribution from exsolution is needed to overcome thermal stratification, but thermal buoyancy exceeds exsolution, so the regime name is somewhat semantic—both buoyancy sources together must overcome the stratification. For $Q_{cmb} \geq 12$ TW, both exsolution and thermal buoyancy contribute to the convection, although exsolution is no longer necessary (red in Figure 4). The main implication of Figure 4 is that even though exsolution can help drive a dynamo over a modest range of subadiabatic CMB heat flows, thermal buoyancy is larger than exsolution and needs to be close to the adiabatic value for an exsolution-dynamo to be possible. The range of core heat flows over which exsolution is important of 9.2–12 TW is relatively small, implying that if exsolution was important in the past it was relatively short-lived.

In addition to the "new core paradox" of Olson (2013), the core cooling rate is entangled with the "thermal catastrophe" of the mantle (e.g., *Korenaga*, 2008), where the present mantle heat flow and typical cooling laws predict the mantle to be unrealistically hot in the recent past. There are at least two proposed solutions to this problem: (1) invoke a deep internal heat source (in the core or lower mantle) of ~3 TW that slows core and mantle cooling (*Driscoll*, 2016), helping to maintain thermal convection in the core until inner core nucleation around 1 Ga; or (2) invoke that the mantle cooling rate is inversely proportional to mantle temperature (*Korenaga*, 2008), implying that heat loss was lower in the hot early Earth and that some other source (such as exsolution) powered the geodynamo over much of the Earth history. Exsolution does not play a major role in the first scenario as our experimental results predict a low energy contribution of <1 TW by exsolution over time (Du et al., 2017), implying that while exsolution can resolve the new core paradox it does not simultaneously resolve the mantle catastrophe. The feasibility of the second scenario has been demonstrated by O'Rourke and Stevenson (2017). Indeed, we find that exsolution may have driven a dynamo when the core was slightly thermally subadiabatic (Figure 4), but its role is limited to a modest range of cooling rates. In either case, the core must have sustained a relatively high heat flow over much of the Earth history so that the core is not too thermally stratified, and core exsolution may have played a complementary role.

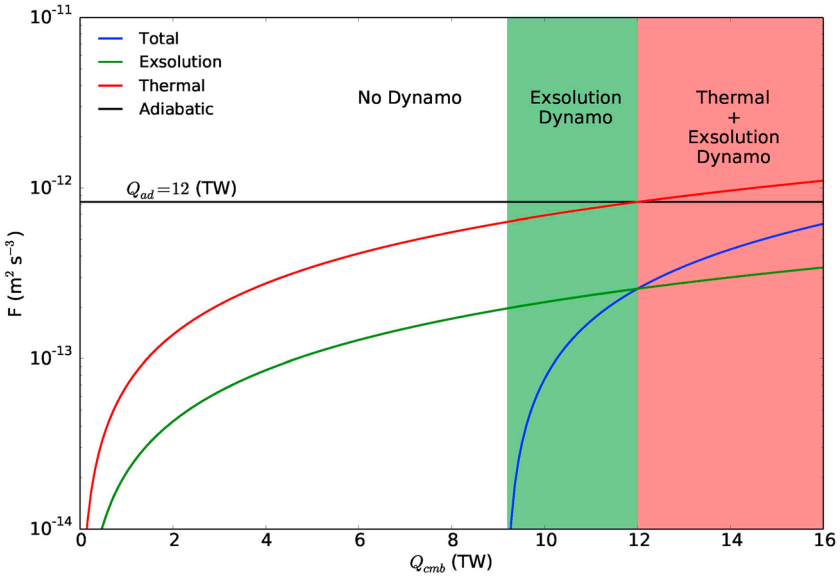

Figure 4. Comparison of core buoyancy fluxes, total (blue), exsolution (green), thermal (red), and adiabatic (black), assuming $Q_{\mathrm{ad}} = 12$ TW ($F_{\mathrm{ad}} = 8.27 \times 10^{-13}$ m^2/s^3) and no core heat sources. For $Q_{\mathrm{cmb}} < 9.2$ TW, the core is stratified (total buoyancy < 0), and no dynamo is expected. For $9.2 \leq Q_{\mathrm{cmb}} \leq 12.0$ TW, exsolution overcomes thermal stratification (total buoyancy flux > 0), and an exsolution-driven dynamo is expected (green shading). For $Q_{\mathrm{cmb}} > 12$ TW, both thermal and exsolution-driven convection and dynamo action are expected (red shading). See supporting information for details.

6. Conclusions and Future Studies

We have conducted new experiments to investigate the partitioning of Mg between Fe alloys and silicate liquids, expanding the temperature range of previous experiments. Like Du et al. (2017), we find that Mg partitioning has a weak temperature dependence and strong oxygen dependence. For nominal core compositions, our results suggest that exsolution may have played a modest role in driving the early geodynamo if the core was not too thermally stratified. However, exsolution does not resolve the thermal catastrophe, implying that an alternative heat source, exotic mantle cooling, or a possible basal magma ocean may be required (Driscoll & Bercovici, 2014; Ziegler & Stegman, 2013). A core enriched in radiogenic elements seems unlikely as indicated by recent experiments and theoretical calculations (e.g., Chidester et al., 2017; Suer et al., 2017; Xiong et al., 2018). A comparison of thermodynamic models demonstrates that exsolution rates are less than 1×10^{-5} K^{-1} and the predicted solubilities of Mg in the core can range from ~0.5 to ~1.5 wt% at the present day. Mg may still be an important light element in the Earth's core and it should be further investigated by future experiments and models.

Acknowledgments
We thank Emma Bullock for electron microprobe analysis at Carnegie Institution of Washington. We appreciate the generosity Jie Li and Jiachao Liu for providing a carbide standard. This manuscript benefited from discussions with Yuan Li, Anat Shahar, Colin Jackson, and James Badro. A. Boujibar thanks the support from Carnegie Fellowship program. This is contribution No.IS-2717 from GIGCAS. This work is supported by grants from Chinese Academy of Sciences and State Key Laboratory of Isotope Geochemistry (No. 29Y93301701, 51Y8340107) to Z. Du, as well as from NSF (EAR-1447311) to Y. Fei. All data used in this paper are in Table S1 and plotted in Figure 1.

References

Badro, J., Aubert, K., Hirose, R., Nomura, I., Blanchard, S. B., & Siebert, J. (2018). Magnesium partitioning between Earth's mantle and core and its potential to drive an early exsolution geodynamo. *Geophysical Research Letters*, *45*, 13,240–13,248. https://doi.org/10.1029/2018GL080405

Badro, J. P., Brodholt, H., Piet, J. S., & Ryerson, F. J. (2015). Core formation and core composition from coupled geochemical and geophysical constraints. *Proceedings of the National Academy of Sciences*, *112*(40), 12,310–12,314.

Badro, J., Siebert, J., & Nimmo, F. (2016). An early geodynamo driven by exsolution of mantle components from Earth's core. *Nature*, *536*(7616), 326–328.

Biggin, A. J., Piispa, E. J., Pesonen, L. J., Holme, R., Paterson, G. A., Veikkolainen, T., & Tauxe, L. (2015). Palaeomagnetic field intensity variations suggest Mesoproterozoic inner-core nucleation. *Nature*, *526*(7572), 245–248.

Chidester, B. A., Rahman, Z., Righter, K., & Campbell, A. J. (2017). Metal–silicate partitioning of U: Implications for the heat budget of the core and evidence for reduced U in the mantle. *Geochimica et Cosmochimica Acta*, *199*, 1–12.

Driscoll, P. E. (2016). Simulating 2 Ga of geodynamo history. *Geophysical Research Letters*, *43*, 5680–5687. https://doi.org/10.1002/2016GL068858

Driscoll, P. E., & Bercovici, D. (2014). On the thermal and magnetic histories of Earth and Venus: Influences of melting, radioactivity, and conductivity. *Physics of the Earth and Planetary Interiors*, *236*, 36–51.

Du, Z., Jackson, C. R. M., Bennett, N., Driscoll, P., Deng, J., Lee, K. K. M., Greenberg, E., et al. (2017). Insufficient energy from MgO exsolution to power early geodynamo. *Geophysical Research Letters*, *44*, 11,376–11,381. https://doi.org/10.1002/2017GL075283

Fischer, R. A., Nakajima, Y., Campbell, A. J., Frost, D. J., Harries, D., Langenhorst, F., et al. (2015). High pressure metal–silicate partitioning of Ni, Co, V, Cr, Si, and O. *Geochimica et Cosmochimica Acta*, *167*, 177–194.

Jackson, C. R. M., Bennett, N. R., Du, Z., Cottrell, E., & Fei, Y. (2018). Early episodes of high-pressure core formation preserved in plume mantle. *Nature*, *553*(7689), 491–495.

Kiseeva, E. S., & Wood, B. J. (2013). A simple model for chalcophile element partitioning between sulphide and silicate liquids with geochemical applications. *Earth and Planetary Science Letters*, *383*, 68–81. https://doi.org/10.1016/j.epsl.2013.09.034

Konopkova, Z., McWilliams, R. S., Gomez-Perez, N., & Goncharov, A. F. (2016). Direct measurement of thermal conductivity in solid iron at planetary core conditions. *Nature*, *534*(7605), 99–101.

Korenaga, J. (2008). Urey ratio and the structure and evolution of Earth's mantle. *Reviews of Geophysics*, *46*, RG2007. https://doi.org/10.1029/2007RG000241

Labrosse, S., Poirier, J.-P., & Le Mouël, J.-L. (2001). The age of the inner core. *Earth and Planetary Science Letters*, *190*(3-4), 111–123. https://doi.org/10.1016/S0012-821X(01)00387-9

Nakajima, M., & Stevenson, D. J. (2015). Melting and mixing states of the Earth's mantle after the Moon-forming impact. *Earth and Planetary Science Letters*, *427*, 286–295. https://doi.org/10.1016/j.epsl.2015.06.023

Ohta, K., Kuwayama, Y., Hirose, K., Shimizu, K., & Ohishi, Y. (2016). Experimental determination of the electrical resistivity of iron at Earth's core conditions. *Nature*, *534*(7605), 95–98. https://doi.org/10.1038/nature17957

Olson, P. (2013). The new core paradox. *Science*, *342*(6157), 431–432.

Olson, P., Landeau, M., & Hirsh, B. H. (2017). Laboratory experiments on rain-driven convection: Implications for planetary dynamos. *Earth and Planetary Science Letters*, *457*, 403–411. https://doi.org/10.1016/j.epsl.2016.10.015

O'Rourke, J. G., & Stevenson, D. J. (2016). Powering Earth's dynamo with magnesium precipitation from the core. *Nature*, *529*(7586), 387–389. https://doi.org/10.1038/nature16495

O'Rourke, J. K., & Stevenson, D. J. (2017). Thermal evolution of Earth with magnesium precipitation in the core. *Earth and Planetary Science Letters*, *458*, 263–272.

Pozzo, M., Davies, C., Gubbins, D., & Alfe, D. (2012). Thermal and electrical conductivity of iron at Earth's core conditions. *Nature*, *485*(7398), 355–358. https://doi.org/10.1038/nature11031

Suer, T.-A., Siebert, J., Remusat, L., Menguy, N., & Fiquet, G. (2017). A sulfur-poor terrestrial core inferred from metal–silicate partitioning experiments. *Earth and Planetary Science Letters*, *469*, 84–97. https://doi.org/10.1016/j.epsl.2017.04.016

Tarduno, J. A., Cottrell, R. D., Davis, W. J., Nimmo, F., & Bono, R. K. (2015). A Hadean to Paleoarchean geodynamo recorded by single zircon crystals. *Science*, *349*(6247), 521–524. https://doi.org/10.1126/science.aaa9114

Wasson, J. T., & Kallemeyn, G. W. (1988). Composition of chondrites. *Philosophical Transaction of the Royal Society of London*, *325*(1587), 535–544. https://doi.org/10.1098/rsta.1988.0066

Xiong, Z., Tsuchiya, T., & Taniuchi, T. (2018). Ab initio prediction of potassium partitioning into Earth's core. *Journal of Geophysical Research: Solid Earth*. https://doi.org/10.1029/2018JB015522

Ziegler, L. B., & Stegman, D. R. (2013). Implications of a long-lived basal magma ocean in generating Earth's ancient magnetic field. *Geochemistry, Geophysics, Geosystems*, *14*, 4735–4742. https://doi.org/10.1002/2013GC005001